Unexpected Hole Transfer Leads to High Efficiency Single-Walled Carbon Nanotube Hybrid Photovoltaic

Nanditha M. Dissanayake and Zhaohui Zhong*

Department of Electrical Engineering and Computer Science, University of Michigan, Ann Arbor, Michigan 48109, United States

ABSTRACT We report surprisingly efficient photocurrent generation at individual single-walled carbon nanotube (SWNT) /poly(3-hexylthiophene-2,5-diyl) (P3HT) junctions. Contrary to previous prediction, both semiconducting SWNTs (s-SWNTs) and metallic SWNTs (m-SWNTs) function as efficient hole acceptors. By active tuning of SWNTs' Fermi level, we confirm that P3HT p-dopes both s-SWNT and m-SWNT, and the work function difference between the nanotube and P3HT leads to a built-in voltage driving the efficient exciton dissociation and hole transfer. We further demonstrate square millimeter scale SWNT/P3HT bilayer photovoltaics using horizontally aligned SWNT arrays. Importantly, the devices exhibit greater than 90% effective external quantum efficiency. These key findings will not only enhance our knowledge of photocurrent generation at nanoscale interfaces, but also make selective omission of m-SWNT redundant, promising carbon nanomaterial-based, low-cost, high-efficiency hybrid photovoltaics.

KEYWORDS Carbon nanotube, P3HT, hybrid photovoltaics, hole acceptor

In organic photovoltaic[1−4] where energy states are discrete, the alignment of the highest occupied molecular orbital (HOMO) and lowest unoccupied molecular orbital (LUMO) across the donor−acceptor interface dictates the exciton dissociation and charge transfer physics.[5−7] This concept has been widely adopted in nanomaterial-based hybrid photovoltaics, including heterojunction devices between one-dimensional systems of single-walled carbon nanotubes (SWNTs)[8,9] and conjugated organic polymers such as poly(3-hexylthiophene-2,5-diyl) (P3HT).[10,11] The HOMO and LUMO alignment of SWNT/P3HT junction predicts that semiconducting (s-) SWNTs are efficient electron acceptors, while metallic (m-) SWNTs create recombination centers impeding charge transfer.[12] Experimental works thus far have been limited to ensemble devices fabricated from blends of SWNTs and polymer, and the existence of m-SWNTs is blamed for the poor overall device performance.[13−17]

To this end, we present a comprehensive experimental investigation of SWNT/P3HT heterojunction containing a single nanotube. Contradictory to conventional belief, our results show that both s-SWNTs and m-SWNTs act as efficient hole acceptors instead of electron acceptors, a result of P3HT p-doping the nanotubes. Furthermore, we demonstrate square millimeter scale SWNT/P3HT bilayer photovoltaics using horizontally aligned SWNT arrays. The effective external quantum efficiency (EQE) after taking into account the exciton diffusion length is measured to be

greater than 90%, promising remarkable potential for solar energy harvesting.

Figure 1a illustrates the schematic of the single junction SWNT/P3HT hybrid photovoltaics. Devices are fabricated on insulating quartz substrates to eliminate the photogating effect, with SWNT contacted by metal electrodes (Al or Pd) and P3HT contacted by transparent indium tin oxide (ITO) (see Supporting Information for details). Atomic force microscopy (AFM) is used to identify devices containing only single nanotube (Figure 1b inset), and solution−gate electrical transport studies[18] are used to identify the semiconducting or metallic nature of SWNTs (Supporting Information Figure S1).

Photoinduced charge transfer is first studied on uniquely identified individual s-SWNT/P3HT and m-SWNT/P3HT junctions, with nanotube length L of 8 μm and Al as the nanotube contact. Here we collect the photocurrent from the ITO side. Under short-circuit condition, s-SWNT/P3HT (Figure 1b, red) and m-SWNT/P3HT (Figure 1b, green) junctions generate −42 pA and −31 pA of photocurrent under an illumination intensity of 1275 mW/cm^2, respectively. Importantly, the sign of photocurrent is negative, indicating hole extraction for both s-SWNT and m-SWNT from P3HT (Figure 1a). As a comparison, the reference Al/P3HT/ITO junction (Figure 1b, black) generates 30 pA of photocurrent in the opposite direction. This positive photocurrent corresponds to electron transfer into Al, agreeing with the lower work function of Al (∼4.3 eV) compared to ITO (∼4.7 eV). Furthermore, a six-SWNT (ensemble of m-SWNTs and s-SWNTs) device shows −130 pA of photocurrent (Figure 1b, blue). The scalable increase of current generation compared to a single junction
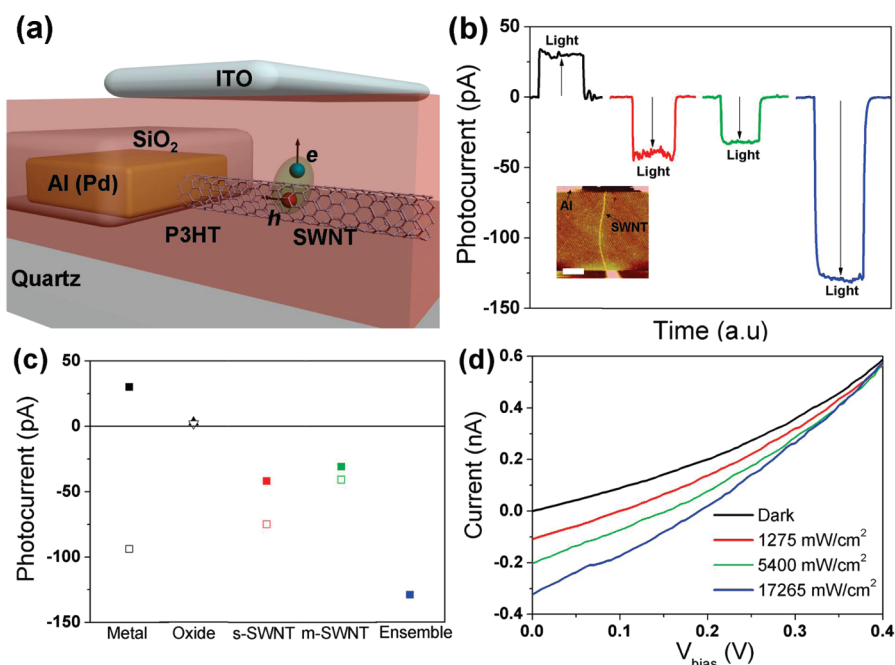
FIGURE 1. Unexpected photocurrent generation at individual SWNT/P3HT heterojunctions reveals both semiconducting and metallic nanotube accepting holes instead of electrons. (a) Schematic of the single junction SWNT/P3HT hybrid photovoltaic. Excitons dissociate at the heterojunction, followed by holes transfer into the nanotube, and electrons collected by ITO electrode. (b) Short circuit photocurrent for an individual s-SWNT/P3HT junction (red line), an individual m-SWNT/P3HT junction (green line), an ensemble SWNT/P3HT device containing six nanotubes (blue line), and an Al/P3HT reference device (Al area of ~1000 um^2) (black line). The devices are under continuous wave (CW) green laser (532 nm) illumination with intensity of 1275 mW/cm^2, and the current is collected from the ITO electrode. (Inset) AFM image of a single SWNT bridging the metal contacts. Scale bar is 2 μm. (c) Short circuit photocurrent of metal/P3HT (black squares), metal/oxide/P3HT (black triangles), single s-SWNT/P3HT (red squares), single m-SWNT/P3HT (green squares), and ensemble SWNT/P3HT (blue square) junctions. Filled and open symbols correspond to Al and Pd electrodes, respectively. (d) Current−voltage characteristics of an Al-contacted ensemble SWNT/P3HT device with six nanotubes under 532 nm CW laser illumination.

once again proves that both m-SWNT and s-SWNT work collectively as hole acceptors.

We further investigate the effect of nanotube contact metal on charge transfer by studying devices with a Pd electrode. As shown in Figure 1c, Pd-contacted individual s-SWNT/P3HT (red open square) and m-SWNT/P3HT junctions (green open square) generate −75 pA and −41 pA of photocurrent, respectively. Importantly, the sign of photocurrent for Pd-contacted devices remains unchanged compared to Al contacted devices (filled squares). For reference Pd/P3HT/ITO junction, we measure a −94 pA photocurrent (black open square). The sign of the photocurrent corresponds to hole transfer into Pd, agreeing with the higher work function of Pd (~5.1 eV) compared to ITO.

These results show that the behavior of the SWNT/P3HT junctions is distinctly different from that of the reference metal/P3HT/ITO junctions. For metal/P3HT/ITO junctions, as expected, photocurrent directions are dictated by the work function difference between metal and ITO. However, for both m-SWNTs and s-SWNTs, hole transfer from P3HT to the nanotube is independent of the contact metal work function, and is solely determined by the SWNT/P3HT heterojunction. Moreover, controlled devices with identical design except SWNTs, i.e., Al/SiO$_2$/P3HT/ITO (black filled-triangle) and Pd/SiO$_2$/P3HT/ITO (black open-triangle), show

negligible photocurrent (Figure 1c, oxide), again confirming that the photocurrent is generated at the SWNT/P3HT heterojunction.

Current−voltage (I−V) behavior under dark and at varying optical illuminations is also characterized, and measurements taken on the six-SWNTs/P3HT junction is shown in Figure 1d. Forward rectifying I−V under dark conditions suggests the formation of heterojunction with higher work function at the nanotube side (Supporting Information Figure S2). Photocurrent increases in the fourth quadrant with increasing light intensity, with an open circuit voltage (V_{oc}) up to 0.2 V under 17.265 W/cm^2 illumination. Furthermore, I−V curves under dark and light conditions merge at ~0.4 V, at which voltage no photocurrent is generated. Importantly, at this bias the energy band can be assumed flat, yielding an estimation of the built-in voltage as ~0.4 V.

To understand the physical mechanism governing the unexpected hole transfer from P3HT to the SWNTs, we fabricate similar devices as in Figure 1a on degenerate doped Si wafers with 300 nm of SiO$_2$. The Si substrate serves as global back gate to electrostatically vary the Fermi level and doping of nanotubes. First, nanotube conductance (G) versus silicon back gate voltage (V_g) is measured before and after the spin-coating of P3HT (Figure 2a). Interestingly, the G−V_g transfer curve shifts to a positive V_g value by 13.1 V after
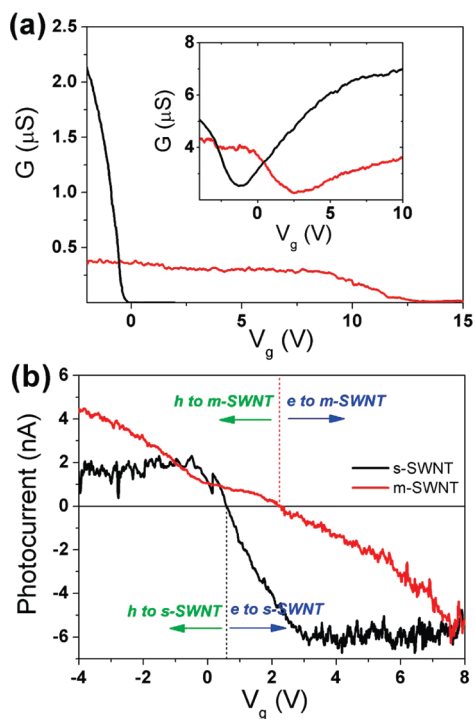
FIGURE 2. P3HT induced p-doping on both s-SWNT and m-SWNT. (a) The G vs V_g curves of an s-SWNT device before (black line) and after (red line) P3HT coating. (Inset) G vs V_g curves of an m-SWNT device before (black line) and after (red line) P3HT coating. The devices are fabricated on silicon substrate with 300 nm SiO_2, and nanotubes are contacted with Pd electrodes. (b) Short circuit photocurrent vs V_g of individual s-SWNT/P3HT (black) and m-SWNT/P3HT (red) devices under 30.3 W/cm^2 532 nm CW laser illumination. The current is collected from the Pd source electrode while keeping ITO at zero bias and floating Pd drain electrode. Positive (negative) photocurrent indicates hole (electron) transfer from P3HT to the SWNTs.

P3HT coating. Similar shift (3.7 V) is also observed for a single m-SWNT device (Figure 2a, inset). The large positive shifts of transfer curves reveal that both s-SWNT and m-SWNT are heavily p-doped. Reports in literature have also shown that organic and organometallic molecules can be used to selectively p-(n-)dope SWNTs,[19,20] but was hitherto unreported in SWNT/P3HT interfaces.

Results from the electrical transport measurements above hint that hole extraction from the SWNT/P3HT junction is closely related to the doping of SWNTs. Thus, we directly measured the photocurrent dependence on nanotube doping by tuning SWNTs' Fermi level using the silicon back gate (Figure 2b). Here we collect current from the Pd source electrode of the SWNTs, with the ITO electrode kept at zero bias and the Pd drain electrode floating. Interestingly, as V_g is swept from −4 to 8 V, photocurrent collected from both the s-SWNT/P3HT junction (black curve) and the m-SWNT/P3HT junction (red curve) change sign. On the basis of our measurement scheme, positive (negative) photocurrent indicates hole (electron) transfer from P3HT to nanotubes. Therefore, both s-SWNTs and m-SWNTs function as hole acceptors at zero or negative gate voltage. However, as V_g

increases to higher positive value, electrostatically induced n-doping overcomes the P3HT p-doping, and both s-SWNTs and m-SWNTs function as electron acceptors.

Our electrical transport measurements, and in particular, gate-dependent photocurrent measurements shine light on the fundamental photocurrent generation mechanism. Exciton dissociation and charge transfer at the SWNT/P3HT junction depend on the work function difference between the nanotube and P3HT. Heavy p-doping of both m-SWNTs and s-SWNTs by P3HT coating increases the nanotube work function. A built-in voltage is developed across the SWNT/P3HT junction with the nanotube at lower potential, resulting in exciton dissociation and hole transfer into nanotubes. The magnitude of the built-in voltage is measured to be ∼0.4 V by the flat-band voltage shown in Figure 1d. This built-in voltage shows close agreement with the difference between the P3HT work function (4.4 eV)[21] and the ionization potential of the SWNT (4.7 eV),[22] which can be approximated to the work function of heavily p-doped SWNTs. Since the exciton binding energy of P3HT is approximately 0.3 eV, the above-mentioned built-in voltage would be adequate for exciton dissociation and photocurrent generation.[23]

To gauge the efficiency of photon-to-current conversion at the SWNT/P3HT junction, we fabricated and measured prototype large-area SWNT/P3HT bilayer photovoltaics. As shown in Figure 3a, devices are fabricated on a monolayer of horizontally aligned SWNT arrays (∼1 tube/μm) grown on quartz substrates[24] with Pd (or Al) finger electrodes as contacts. Figure 3b shows wavelength-dependent photocurrent measurements from a 1 mm^2 device with 3 μm SWNT channel length. Larger photocurrent is obtained at a photon wavelength of 350−600 nm, suggesting that photocurrent generation is due to light absorption in the P3HT. The EQE, calculated by taking the ratio between the number of extracted free charges to the number of incident photons at each wavelength, shows a maximum of 0.37 % at 390 nm. The low EQE is expected since exciton dissociation only occurs though a monolayer of SWNTs. Given the small exciton diffusion length in P3HT, Λ_E ∼8.5 ± 0.7 nm,[25] the majority of excitons recombine before arriving at the SWNT/P3HT heterojunction.

In order to evaluate the intrinsic loss at the heterojunction, we further calculate the effective EQE by considering the effective volume of photon absorption/dissociation near the SWNT/P3HT junctions. Since the SWNTs are geometrically aligned, the effective volume of each heterojunction can be estimated as a rectangular box having a width of 17 nm (twice that of Λ_E), length of 3 μm (SWNT length), and height of the 8.5 nm (Λ_E) (Figure 3c, inset). Therefore, the effective EQE can be estimated by taking the ratio of the number of free carriers to the number of photons incident within the effective device volume (see Supporting Information for details). Significantly, we measured an effective EQE exceeding 90 % at 405 nm, and greater than 50 % between 358 to 472 nm (Figure 3c). We also note that the main error of
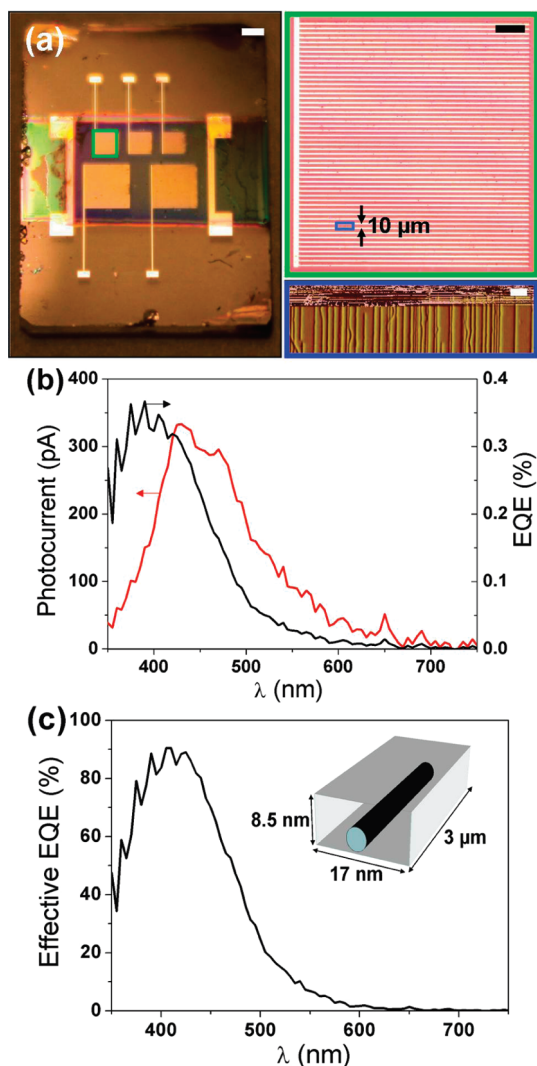
FIGURE 3. Large area SWNT/P3HT bilayer hybrid photovoltaics show larger than 90% effective EQE. (a) Optical image of the large area devices fabricated on a quartz substrate. Scale bar is 1 mm. (Green box) A magnified image of the 1 mm² device with a 10 μm nanotube channel length. Scale bar is 100 μm. (Blue box) An AFM image of a horizontally aligned SWNT array. Scale bar is 2 μm. (b) Wavelength-dependent short circuit photocurrent (red curve, left axis) and EQE (black curve, right axis). Data taken from a 1 mm² device with 3 μm nanotube channel length, with integrated illumination intensity of 96 mW/cm². (c) Estimated effective EQE of the same device. Only those excitons that arrive at the heterojunctions can contribute to the photocurrent. (Inset) Effective volume of a single junction estimated as a rectangular box having a width of 17 nm (twice that of Λ_E), length of 3 μm (SWNT length), and height of 8.5 nm (Λ_E).
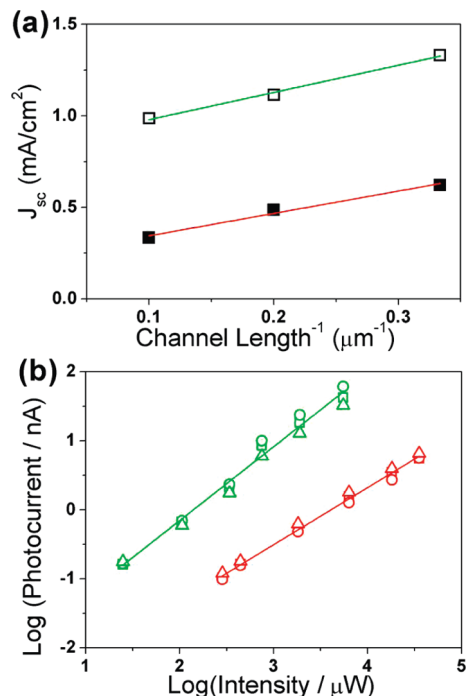

FIGURE 4. SWNT/P3HT illumination intensity dependence of the photocurrent. (a) Photocurrent density vs reciprocal SWNT channel length for the large-area (1 mm²) devices with Al (filled symbols) and Pd (open symbols) electrodes. Short circuit photocurrent measurements were carried out under AM1.5G illumination. Lines are the linear fits. (b) Photocurrent vs illumination intensity for the large area devices under 532 nm (green symbols) and 800 nm (red symbols) illumination. The SWNT channel lengths are 3 μm (square), 5 μm (circle) and 10 μm (triangle), respectively. Lines are the linear fits.

our effective EQE calculation comes from Λ_E estimation. From literature,[25] Λ_E is measured to be 8.5 ± 0.7 nm, yielding an effective EQE uncertainty of ±7.5%. Nevertheless, these results demonstrate extremely efficient photon harvesting capability without the need of excluding m-SWNTs, thus promising remarkable potential for nanotube-based hybrid photovoltaics.

Next, we studied the effect of SWNT channel length on photocurrent generation. Figure 4a shows that the short circuit current density J_{sc} is inversely proportional to SWNT channel lengths for both Al (filled squares) and Pd (open squares) contacted devices. At room temperature and micrometer length scale, both m-SWNTs and s-SWNTs are diffusive conductors with conductance scales as $1/L$. With SWNT/P3HT heterojunction arrays acting as power generators in parallel, the photocurrent thus scales with SWNT channel conductance as $1/L$.

Last, we investigated the exciton loss mechanism by studying photocurrent dependence on illumination intensity for devices with 3, 5, and 10 μm SWNT channel lengths. Log−log plots of short circuit photocurrent (I_{sc}) versus illumination intensity (P) are shown in Figure 4b. Under 532 nm monochromatic illumination, I_{sc} increases linearly with P for devices with L = 3, 5, and 10 μm. Importantly, such linear power dependence agrees with negligible bimolecular recombination, suggesting fast carrier extraction from the heterojunction even for 10 μm long SWNT channels.[26] In addition, a sublinear dependence of $I_{sc} \sim P^{0.8}$ is observed under 800 nm illumination. It is believed that dissociation of low-energy exciton creates trapped negative polarons in P3HT, leading to stronger charge recombination.[27]

We believe that fast carrier extraction plays important role for the extremely efficient photocurrent generation in our SWNT/P3HT hybrid devices. The time scale for hole

extraction can be estimated as the free carrier traveling length ($L/2$) divided by the drift velocity. With nanotube hole mobility $\mu_h \sim 10\,000$ cm^2 V^{-1} s^{-1}[28] and built-in voltage $V_{bi} \sim 0.4$ V, the order of magnitude hole extraction time for the $L = 10$ μm device can be calculated as $(L/2)^2/(\mu_h \times V_{bi}) \sim 62$ ps. Unlike previous designs, where nanotubes are blended with polymer, direct contacting to each individual nanotube thus ensures complete extraction of carriers before they recombine. Our findings also eliminate constrain of selective synthesis/sorting of s-SWNTs, paving the way for low-cost manufacturing. Furthermore, 100% absorption of incident illumination could be possible by adopting multilayer SWNTs or using vertically aligned SWNT arrays[29] interpenetrated with the polymer. Finally, our techniques can be readily applied to investigate other types of nanomaterial/polymer systems for future-generation, cost-efficient hybrid photovoltaics.

Supporting Information Available. Device fabrication, electrical and optical characterizations, effective EQE calculation of the SWNT/P3HT device, figures for solution gate measurement of semiconducting and metallic SWNTs, dark $I-V$ measurement, schematic illustration of the model used for the effective EQE calculation, and the absorption coefficient measurement of P3HT thin film. This material is available free of charge via the Internet at http://pubs.acs.org.

REFERENCES AND NOTES

(1) Sun, S.; Sariciftci, N. S. *Organic Photovoltaics: Mechanisms, Materials and Devices*; CRC Press: Boca Raton, FL, 2005.

(2) Yu, G.; Gao, J.; Hummelen, J. C.; Wudl, F.; Heeger, A. J. *Science* **1995**, *270*, 1789–1791.

(3) Park, S. H.; Roy, A.; Beaupre, S.; Cho, S.; Coates, N.; Moon, J. S.; Moses, D.; Leclerc, M.; Lee, K.; Heeger, A. J. *Nat. Photonics* **2009**, *3*, 297–302.

(4) Forrest, S. R. *Mater. Res. Soc. Bull.* **2005**, *30*, 28–32.

(5) Gregg, B. A.; Hanna, M. C. *J. Appl. Phys.* **2003**, *93*, 3605–3614.

(6) Peumans, P.; Yakimov, A. *J. Appl. Phys.* **2003**, *93*, 3693–3723.

(7) Blom, P. W. M.; Mihailetchi, V. D.; Koster, L. J. A.; Markov, D. E. *Adv. Mater.* **2007**, *19*, 1551–1566.

(8) Saito, R.; Dresselhaus, G.; Dresselhaus, M. S. *Physical Properties of Carbon Nanotubes*; Imperial College Press: London, 1998.

(9) Garbor, N. M.; Zhong, Z.; Bosnick, K.; Park, J.; McEuen, P. L. *Science* **2009**, *325*, 1367–1371.

(10) Sirringhaus, H.; Brown, P. J.; Friend, R. H.; Nielsen, M. M.; Bechgaard, K.; Langeveld-Voss, B. M. W.; Spiering, A. J. H.; Janssen, R. A. J.; Meijer, E. W.; Herwig, P.; de Leeuw, D. M. *Nature* **1999**, *401*, 685–687.

(11) Kim, Y.; Cook, S.; Tuladhar, S. M.; Choulis, S. A.; Nelson, J.; Durrant, J. R.; Bradley, D. D. C.; Giles, M.; McCulloch, I.; Ha, C. S.; Ree, M. *Nat. Mater.* **2006**, *5*, 197–203.

(12) Kanai, Y.; Grossman, J. C. *Nano Lett.* **2008**, *8*, 908–912.

(13) Romero, D. B.; Carrard, M.; de Heer, W.; Zuppiroli, L. *Adv. Mater.* **1996**, *8*, 899–902.

(14) Harris, P. J. F. *Int. Mater. Rev.* **2004**, *49*, 31–43.

(15) Schuettfort, T.; Nish, A.; Nicholas, R. J. *Nano Lett.* **2009**, *9*, 3871–3876.

(16) Pasquier, A. D.; Unalan, H. E.; Kanwal, A.; Miller, S.; Chhowalla, M. *Appl. Phys. Lett.* **2005**, *87*, 203511.

(17) Geng, J.; Zeng, T. *J. Am. Chem. Soc.* **2006**, *128*, 16827–16833.

(18) Rosenblatt, S.; Yaish, Y.; Park, J.; Gore, J.; Sazonova, V.; McEuen, P. L. *Nano Lett.* **2002**, *2*, 869–872.

(19) Shim, M.; Javey, A.; Kam, N. W. S.; Dai, H. *J. Am. Chem. Soc.* **2001**, *123*, 11512–11513.

(20) Takenobu, T.; Takano, T.; Shiraishi, M.; Murakami, Y.; Ata, M.; Kataura, H.; Achiba, Y.; Iwasa, Y. *Nat. Mater.* **2003**, *2*, 683–688.

(21) Wu, M.; Lin, Y. Y.; Chen, S.; Liao, H. C.; Wu, Y. J.; Chena, C. W.; Chen, Y. F.; Su, W. F. *Chem. Phys. Lett.* **2009**, *468*, 64–68.

(22) Okazaki, K.; Nakato, Y.; Murakoshi, K. K. *Phys. Rev. B* **2003**, *68*, No. 035434.

(23) Alvarado, S. F.; Seidler, P. F.; Lidzey, D. G.; Bradley, D. D. C. *Phys. Rev. Lett.* **1998**, *81*, 1082.

(24) Kang, S. J.; Kocabas, C.; Ozel, T.; Shim, M.; Pimparkar, N.; Alam, M. A.; Rotkin, S. V.; Rogers, J. A. *Nat. Nanotechnol.* **2007**, *2*, 230–236.

(25) Shaw, P.; Ruseckas, A.; Samuel, I. D. W. *Adv. Mater.* **2008**, *20*, 3516–3520.

(26) Kymakis, E.; Kornilios, N.; Koudoumas, E. *J. Phys. D: Appl. Phys.* **2008**, *41*, 165110.

(27) Nelson, J.; Choulis, S. A.; Durrant, J. *Thin Solid Films* **2004**, *451*, 508–514.

(28) Zhou, X.; Park, J. Y.; Huang, S. M.; Liu, J.; McEuen, P. L. *Phys. Rev. Lett.* **2005**, *95*, 146805.

(29) Hata, K.; Futaba, D. N.; Mizuno, K.; Namai, T.; Yumura, M.; Iijima, S. *Science* **2004**, *306*, 1362–1364.